Solvation-induced cluster anion core switching from $NNO_2^-(N_2O)_{n-1}$ to $O^-(N_2O)_n$

Kostyantyn Pichugin, Emily Grumbling, Luis Velarde, and Andrei Sanov[a)]
Department of Chemistry, University of Arizona, Tucson, Arizona 85721-0041, USA

(Received 16 May 2008; accepted 19 June 2008; published online 28 July 2008)

We report a photoelectron imaging study of the $[O(N_2O)_n]^-$, $0 \leq n \leq 9$, cluster anions generated via electron bombardment of a pulsed supersonic expansion of pure N_2O gas. Depending on cluster size, the photoelectron image features and spectral trends, examined at 355 and 266 nm, give evidence of two dominant core-anion structures, corresponding to the $NNO_2^-(N_2O)_{n-1}$ and $O^-(N_2O)_n$ cluster anions. In agreement with previous studies, the $n=1$ anion has a covalently bound (Y-shaped) NNO_2^- structure. The NNO_2^- core is also found to persist in the larger clusters, up to $n=3$. However, for $n \geq 4$ (and up to at least $n=9$) signatures of an O^- core are predominantly observed. Photofragmentation studies at 355 nm support these results. © *2008 American Institute of Physics*. [DOI: 10.1063/1.2956834]

I. INTRODUCTION

Clusters have long been utilized for studying the microscopic details of intermolecular interactions.[1,2] In particular, the cluster-anion series $X^- \cdot M_n$, where X^- is the core anion and M is the solvent, allow for a molecule-by-molecule evaluation of a solvent's effect on the energy and structure of a charged solute.

The structures and energetics of such systems can be elucidated by photoelectron spectroscopy.[1,2] It is well understood that solvated anions are usually stabilized by ion-neutral interactions. On a pairwise basis, these mostly electrostatically controlled interactions tend to be weaker than the covalent bonds in either the solute or the solvent, but their combined effect for many solvent molecules (and generally accounting for the many-body interactions)[3] can easily exceed a typical covalent bond energy. To the contrary, the corresponding neutral states are usually stabilized to a much lesser degree due to the weaker strength of van der Waals bonding. As a result, solvation tends to increase the vertical detachment energy (VDE) of anionic species. In the absence of chemical rearrangements, the increase is expected to be gradual and monotonic with the number of solvating molecules. Discontinuities in this trend usually signal abrupt changes in the structure of the core anion.

A classic example of such behavior was reported by DeLuca *et al.*[4] for the $(CO_2)_n^-$, $n=2-13$ cluster series, later expanded by Tsukuda *et al.*[5] for the $n=2-16$ range. The photoelectron spectra of the size-selected $(CO_2)_n^-$ cluster anions obtained by these authors display two different photodetachment band series: one corresponding to higher VDEs is observed for the $n=2-6$ and $n=14$ clusters, and the other, with lower VDEs, is observed in the $n=6-13$ range. The VDE discontinuities at $n=6$ and 14 cannot be accounted for by ordinary solvation and are attributed to structural changes in the cluster core. Specifically, these changes have been described as a core switching (at $n=6$) from the covalent dimer anion $(O_2CCO_2)^-$, whose structure was originally proposed by Fleischman and Jordan,[6] to the monomer CO_2^- and back (at $n=14$).[4,5]

Another study by Tsukuda *et al.*[7] revealed a similar phenomenon for $(NO)_n^-$. For this cluster series, the VDE was found to increase by nearly 0.8 eV from $n=2$ to $n=3$, while only moderate consecutive increases (~0.1 eV) were observed in the $n=3-7$ range. The VDE trend for $n=3-7$ is consistent with stepwise solvation of a charged cluster core, but the abrupt changes occurring between $n=1$ and 2 and between $n=2$ and 3 once again signal structural changes in the core anion. In this case, a gradual assembly (or building up) of the core anion is observed as the $(NO)_n^-$ cluster size increases. Specifically, the core anions in these clusters are described as (obviously) NO^- for $n=1$, a covalently bound dimer anion for $n=2$, and (preferentially) a covalently bound *trimer* anion for $n=3$. That is, in the $n \leq 3$ range, the excess electron delocalizes between all available NO moieties. In larger clusters, the size of the anionic core no longer increases with n and the additional NO molecules play the role of neutral solvents.[7]

Multiple isomeric forms of $N_2O_2^-$ have been the subject of an increasing number of studies,[8–14] in part due to the interest in the possible role of their neutral analogs as intermediates in atmospheric processes.[14] Posey and Johnson, using pulsed supersonic expansion of distinct precursor gas mixtures ionized by a fast electron beam, identified three distinct forms of $N_2O_2^-$: (i) the $O_2^- \cdot N_2$ ion-molecule complex, observed in the expansion of O_2 seeded in nitrogen; (ii) the C_{2v} symmetry Y-shaped NNO_2^- anion (analogous to CO_3^-), formed in the expansion of pure N_2O; and (iii) an NO dimer anion, *cis*- or *trans*-$ONNO^-$, generated by seeding NO in the Ar carrier gas.[8] In this work, we are primarily concerned with the Y-shaped (NNO_2^-) isomer[8,10,12,14] and changes in its structure under solvation by N_2O.

Dissociative electron attachment to N_2O is understood to be a preliminary step in the formation of NNO_2^- in electron-

[a)]Electronic mail: sanov@u.arizona.edu.

impact anion sources.[15–24] This process yields N_2 and O^- and in the presence of third bodies may be followed by the $O^- + N_2O \rightarrow NNO_2^-$ association reaction.[8] Such processes in neutral N_2O clusters have been shown to yield an anionic cluster series, often termed $O^-(N_2O)_n$.[16,17,20,21,24–26] In the thermodynamics study on this series for $n=2-7$, Hiraoka *et al.*[25] suggested an $NNO_2^-(N_2O)_{n-1}$ structural form for these clusters. Based on the accepted NNO_2^- structure for the $n=1$ member of this cluster series, they also suggested that the first effective solvent shell in $NNO_2^-(N_2O)_{n-1}$ is completed at $n=3$, corresponding to preferential solvation of the two equivalent anionic oxygen sites.

Here, we report a spectroscopic study of the mass-selected $[O(N_2O)_n]^-$, $n=0-9$ cluster anions by way of photoelectron imaging.[27,28] We identify covalently bound NNO_2^- as a core anion in the small $(n=1-3)$ clusters, while in the larger $(n>3)$ clusters O^- is determined to be the dominant ionic core. We argue that the strong solvation interactions involving the more localized charge distribution of the atomic anion may provide for preferential stabilization of O^- in the larger clusters. These results further demonstrate a solvent's ability to affect chemical structure and highlight the utility of photoelectron imaging for characterizing such phenomena.

II. EXPERIMENTAL APPARATUS

The photoelectron imaging apparatus used in this study is described in detail elsewhere.[29] It employs the techniques of pulsed ion spectroscopy,[30] combined with velocity-map[31] imaging[32] detection of photoelectrons.

The $[O(N_2O)_n]^-$ clusters are formed by expansion of pure N_2O gas at a stagnation pressure of 2.5 atm through a pulsed supersonic nozzle (General Valve Series 9) operated at a repetition rate of 50 Hz into a high-vacuum chamber with a base pressure of 10^{-6} Torr (rising to $(6-8)\times10^{-5}$ Torr when the valve is operated). A focused 1 keV electron beam, propagating counter to the supersonic expansion, is directed straight into the nozzle's throat. This arrangement has been shown by the Johnson group to favor the production of larger clusters,[33] while the use of pure N_2O as a precursor gas should favor the formation of the *Y*-shaped NNO_2^- isomer.[8] The anions are pulse extracted into a Wiley–McLaren[34] time-of-flight mass spectrometer, accelerated to about 2.5 keV, and focused using an Einzel lens.[35] After entering the detection region of the instrument with a base pressure of $(3-5)\times10^{-9}$ Torr, the ions are detected with mass-resolution using a dual-microchannel-plate (MCP) detector (Burle, Inc.) mounted at the end of the mass-spectrometer's flight tube.

Photoelectrons are produced by intersecting the mass-selected cluster ions of interest with a linearly polarized laser beam. The third and fourth harmonics of the Nd:YAG (yttrium aluminum garnet) laser (Spectra Physics Inc., model Laboratory 130–50) are used as sources of the 355 and 266 nm radiations, respectively. When necessary, in order to enhance signal-to-noise ratio of a photoelectron signal, the laser beam is mildly focused with a lens (2.0 m focal length), positioned 1.3 m before the laser and ion beam crossing. Photoelectrons are extracted by a static electric field in the velocity-map[31] imaging assembly through an electron flight tube, internally shielded with μ-metal, and onto a 40 mm MCP detector with a P47 phosphor screen (Burle, Inc.). To minimize backgrounds, the potential difference across the two imaging MCPs, normally maintained at 1.0–1.2 kV, is pulsed up to 1.8 kV for the 250 ns window coinciding with the arrival of photoelectrons. The signal from the phosphor screen is recorded with a charge-coupled device camera (CoolSnap, Roper Scientific, Inc.) and typically accumulated for $(1-5)\times10^5$ experimental cycles. A photoelectron image is a two dimensional projection of the three dimensional photoelectron probability distribution on the plane of the detector. Owing to the cylindrical symmetry imposed by the linear laser polarization (parallel to the detector plane), the speed, and angular distributions of the photoelectrons can be reconstructed via inverse Abel transform.[36] Abel inversion is performed using the BASEX (basis set expansion) program.[37]

Supplementary photofragmentation studies are carried out on a separate negative-ion spectrometer,[38] which employs similar ion-generation and mass-selection techniques. The third-harmonic output of the same Nd:YAG laser (355 nm, 15 mJ) is focused to an ~5 mm diameter spot size at the intersection with the ion beam. The resulting photofragments are analyzed using a single-stage reflectron mass spectrometer and detected with a secondary (off-axis) MCP detector.

III. RESULTS

In this section, we present photoelectron imaging and photofragmentation results for the $[O(N_2O)_n]^-$, $n=0-9$ cluster anion series. Figure 1 shows the 355 nm results (both photoelectron imaging and cluster fragmentation), while Fig. 2 displays the 266 nm data (photoelectron imaging only).

The raw photoelectron images and the corresponding spectra shown in Figs. 1 and 2 are hereafter referred to as data sets 1.*n* and 2.*n*, respectively, with $n=0-9$ referring to the $[O(N_2O)_n]^-$ cluster size. Each photoelectron image shown is the sum of multiple collections, corresponding to a total of $(1-5)\times10^5$ experimental cycles. All images for a given wavelength are displayed on the same velocity scale. The intensity scales are chosen arbitrarily to highlight the most relevant features of the individual images; therefore, they do not reflect the absolute cross sections. The $O(^3P, {}^1D) \leftarrow O^-(^2P)$ photodetachment transitions[39] in data sets 1.0 and 2.0 were used for electron kinetic energy (eKE) calibration of the rest of the data. Although the fine structure of the transitions is not resolved in the present case, photoelectron imaging is capable of such resolution, as demonstrated recently by Cavanagh *et al.*[40]

To elucidate the two-photon character of some of the observed transitions, separate 355 nm photodetachment experiments were carried out with unfocused and slightly focused laser beams, corresponding to average fluences of 1.1×10^6 and 3.7×10^6 W/cm^2, respectively. Figure 1 displays the 355 nm results obtained under one or the other set of conditions. In particular, images 1.0 and 1.4–1.9 correspond to the low power density, while images 1.1–1.3 were

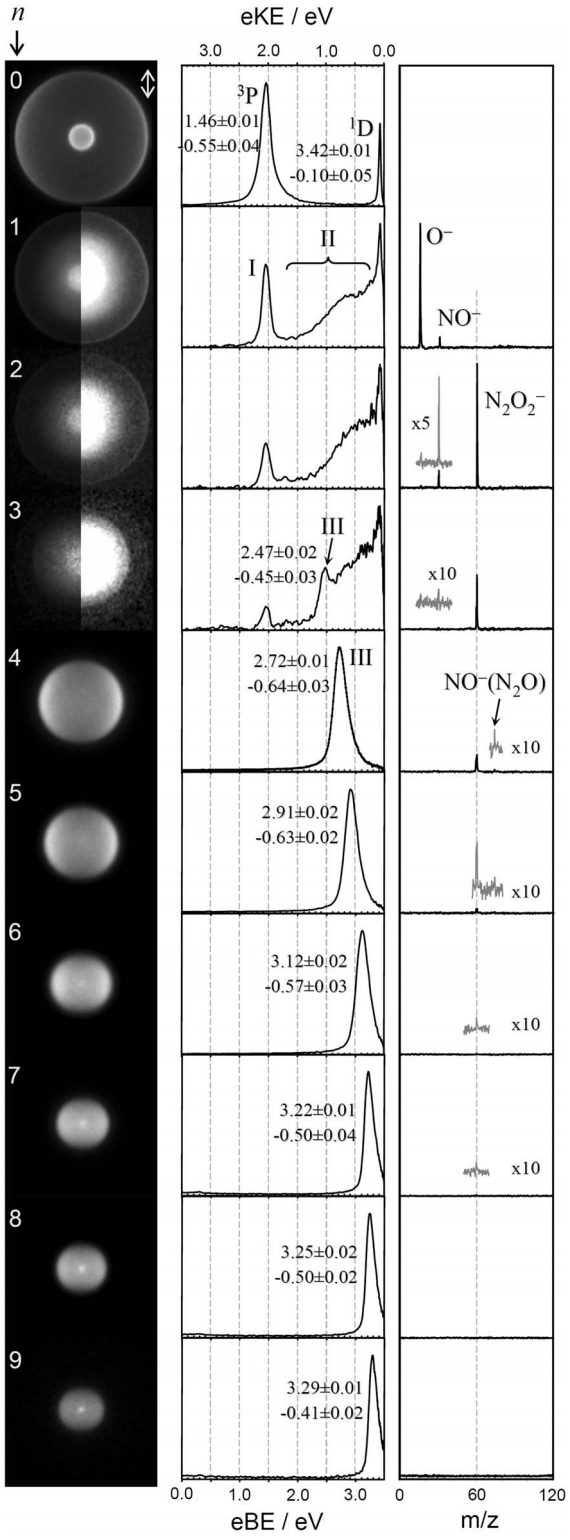

FIG. 1. Photoelectron images (left column), the corresponding photoelectron spectra (middle column), and photofragment-ion mass spectra (right column) for the $[O(N_2O)_n]^-$, $n=0-9$ cluster anion series obtained at 355 nm. The vertical double arrow in the $n=0$ photoelectron image defines the laser polarization axis for all images. All images are shown on the same velocity scale. The photoelectron spectra are normalized to the corresponding maximum intensities. The vertical detachment energies along with anisotropy parameters for bands with clearly defined maxima are indicated next to the corresponding spectral features. See the text for band assignments and further details. The photofragmentation spectra are normalized relative to the parent-ion intensity for each species, so that their decreasing relative intensities reflect the corresponding diminishing photofragmentation cross sections.

recorded with the higher flux. The high-flux images are shown in split scale, highlighting different-intensity features. All 266 nm images (Fig. 2) were collected with a mildly focused laser beam of 1.0×10^6 W/cm^2 fluence.

Overall, the photoelectron images and the corresponding spectra in Figs. 1 and 2 include two types of features. The first are narrow bands, suggestive of atomic or atomiclike transitions. Others exhibit broader and more complex structures, as typically seen in detachment from molecular anions. These features, as well as energetic and angular considerations, provide the basis for structural characterization of each cluster species. The vertical detachment energies for bands with clearly defined maxima are indicated in Figs. 1 and 2 next to the corresponding spectral features. The second values, shown just below the VDEs, are the anisotropy parameters (β_2) determined for the corresponding transitions.

The 355 nm photoelectron images. The unsolvated O^- photoelectron spectrum at 355 nm (Fig. 1.0) shows two peaks corresponding to the $O(^3P,\ ^1D)\leftarrow O^-(^2P)$ transitions with the detachment energies of 1.46 and 3.42 eV, respectively. Similar features (without any measurable solvation-induced shifts) are also present in data sets 1.1–1.3. The intensities of these signals increase relative to other spectral features upon slight focusing of the laser beam. (Accordingly, in Fig. 1 we have chosen to display the higher-flux results for $n=1-3$, in order to accentuate the O^- features.) This nonlinear behavior indicates that the unshifted O^- transitions in $[O(N_2O)_n]^-$, $n=1-3$ result from a two-photon process, ascribed to the photodissociation of the $N_2O_2^-$ cluster core and evaporation of solvent molecules, followed by O^- fragment photodetachment. This nonlinear behavior was not observed for the other transitions in the same spectra.

For brevity, we will refer to these two-photon bands as type I transitions. Similar O^- fragment signatures were seen in the previous studies of NNO_2^- at 532 and 266 nm,[8,12] as well as in the photoelectron spectroscopy studies of the $ONNO^-$ isomer at 355 and <420 nm.[7,8] As discussed in the Introduction, past experiments under similar ion-source conditions have yielded almost exclusively the covalent, *Y*-shaped (NNO_2^-) isomer of $N_2O_2^-$.[8,12] This isomer is expected to be dominant among the $n=1$ species in our experiment. Although the 355 nm photon energy is insufficient for direct detachment of *Y*-shaped NNO_2^-,[12] the observed type I signals are consistent with its photodissociation, followed by O^- fragment photodetachment. In addition to the type I transitions, data set 1.1 contains a broad band labeled II. This feature is ascribed to direct photodetachment of the $ONNO^-$ isomer,[7,8,13] which is also present in the ion beam.

For $n=2$ and 3 (Figs. 1.2 and 1.3, respectively), type I (O^- fragment) features are also observed, as well as analogs of band II. While the former do not show any solvation-induced shift, band II moves to progressively higher binding energies as n increases, consistent with solvent stabilization of the $ONNO^-$ anion. These observations suggest similar molecular-anion core structures persisting in the $n=1-3$ cluster size range. However, Fig. 1.3 ($n=3$) contains an additional peak (labeled III) at eBE=2.47 eV.

The $n=4-9$ data are similar to $n=0$ in that we noticed no changes in the overall structure of the photoelectron spec-

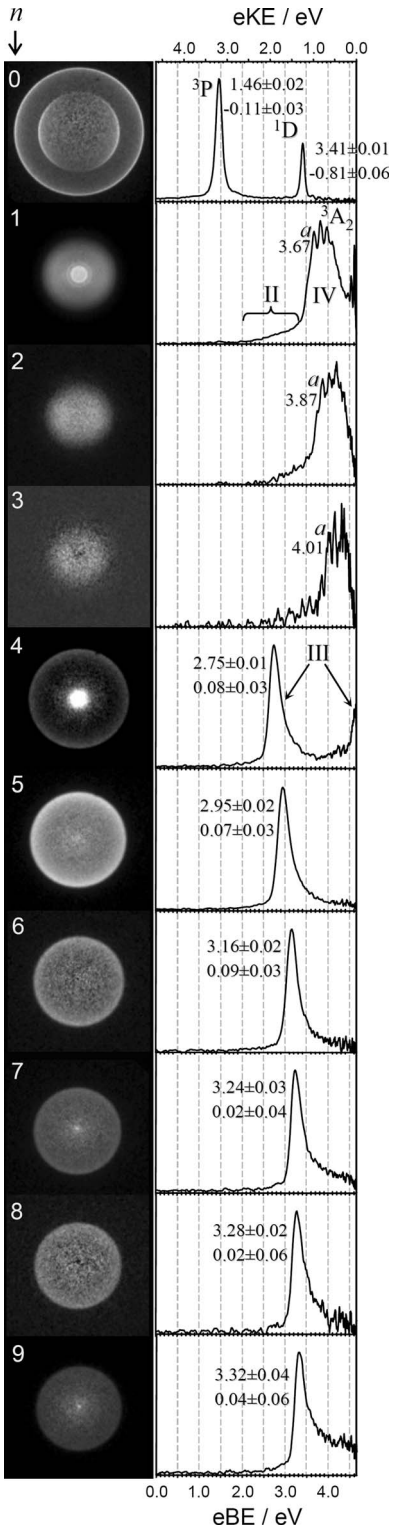

FIG. 2. Photoelectron images and the corresponding photoelectron spectra for the $[O(N_2O)_n]^-$, $n=0-9$ cluster anion series obtained at 266 nm. All images are shown on the same velocity scale. The spectra are normalized to the corresponding maximum intensities. The vertical detachment energies along with anisotropy parameters for bands with clearly defined maxima are indicated next to the corresponding spectral features. See the caption to Fig. 1 and the text for further details and band assignments.

tra with respect to the laser flux conditions. The absolute signal levels are significantly larger for $n=4-9$, compared to $n=1-3$, and the corresponding photoelectron spectra are strikingly different. Each of the larger species exhibits just one intense and relatively narrow (atomiclike) transition, which peaks at progressively higher binding energies as n increases. The comparison of spectra 1.3 and 1.4–1.9 in Fig. 1 suggests that the type III transition, observed for $n=3$, belongs to this progression. For $n=4$ and 5, type III features are centered at eBE=2.72 and 2.91 eV, respectively, compared to 2.47 eV for $n=3$. By interpolation, this spectral series is consistent with $O(^3P) \leftarrow O^-(^2P)$ photodetachment in $O^-(N_2O)_n$, progressively shifted due to the solvation with additional N_2O molecules. The angular distributions of the type III transitions for $n \geq 3$ are also qualitatively similar to the corresponding transition in unsolvated $O^-(n=0)$ at the same wavelength, as reflected by the β_2 values included in Fig. 1.

In summary, the 355 nm photoelectron imaging results suggest a molecular-anion core for the $[O(N_2O)_n]^-$, $n=1-3$ clusters, and an O^- core for $n=4-9$. The exact nature of the covalent core cannot be established based on these data alone, but the results are consistent with both the *Y*-shaped NNO_2^- and $ONNO^-$ isomers identified by Posey and Johnson.[8] Although we expect the NNO_2^- structure to be dominant under the ion-generation conditions employed in the present work, only $ONNO^-$ undergoes direct photodetachment at 355 nm, resulting in band II in the photoelectron spectra shown in Figs. 1.1–1.3.

The 266 nm photoelectron images. In the 266 nm data presented in Fig. 2, a new molecular-type transition (labeled IV) appears for $n=1-3$. Band IV shows partially resolved vibrational structure, particularly clear in data set 2.1, which allows us to identify it as a signature of the *Y*-shaped NNO_2^- anion, arising from detachment to the $^3A_2$ state of the neutral.[12] In order to quantify the solvation-induced shift of band IV, we identify the first (lowest-eBE) vibrational peak (labeled *a*) and use it as a marker (i.e., the detachment energies indicated in Figs. 2.1–2.3 correspond to transition *a*).

The $ONNO^-$ signal (band II, most prominent in data set 2.1) appears as a weak, low-eBE tail of band IV, at a small fraction of the NNO_2^- signal intensity. The two-photon signal from the O^- fragment, seen at 355 nm for $n=1-3$, is not observed at 266 nm. Although its absence may be attributed partially to a smaller 266 nm O^- channel dissociation cross section (compared to 355 nm), we believe that the lower 266 nm laser fluence is primarily responsible for the reduction of the two-photon signal.

We also note that the photoelectron spectrum in Fig. 2.3 contains no band that can be attributed to the O^- cluster core. This may seem surprising, as the 355 nm results clearly indicate the presence of some $O^-(N_2O)_3$ clusters (feature III in spectrum 1.3). However, using band II (arising from the $ONNO^-$ cluster core) as a reference, we do not expect that the signal due to $O^-(N_2O)_3$ in Fig. 2.3 would rise above the noise level.

The 266 nm spectra for the larger clusters ($n>3$) are consistent with those obtained at 355 nm, suggesting atomic-anion (O^-) cluster cores. The VDEs indicated for the type III bands in Figs. 1 and 2 differ only within the experimental uncertainty. For $n=4$, the higher-energy $O(^1D) \leftarrow O^-(^2P)$ photodetachment transition is also observed at a near-zero eKE. This transition is inaccessible for $n>4$ due to the ad-

ditional solvent stabilization. While some of the 266 nm images for $n \geq 7$ do show faint central features (eKE$\approx$0), the corresponding contributions to the photoelectron spectra in the low-eKE range are negligibly small.

The anisotropy parameters determined for the $O^-(N_2O)_n$, $n>3$ clusters at 266 nm (β ranging from 0.02 to 0.08 in Figs. 2.4–2.9) are significantly different from the $\beta = -0.11 \pm 0.03$ value for the corresponding transition in unsolvated O^- (Fig. 2.0). These variations are thought to reflect resonant photoelectron scattering off the N_2O solvent[41] and will be the subject of an upcoming publication.

In summary, the 266 nm photoelectron data indicate the same abrupt change in the $[O(N_2O)_n]^-$ cluster-core structure occurring at $n=4$ as seen in the 355 nm data. The switch from broad molecular transitions in the $n=1-3$ range to atomiclike bands for $n \geq 4$ suggests a molecular-to-atomic anion ($NNO_2^- \rightarrow O^-$) core switching.

355 nm photofragmentation. Also reported in Fig. 1 are the 355 nm photofragment mass spectra for the mass-selected $[O(N_2O)_n]^-$ cluster anions in the $n=1-9$ range. These spectra are acquired under the same laser fluence and normalized to the absolute parent-ion intensities, and therefore can be used to compare the fragmentation yields for different parent anions. The decrease in the overall fragment-ion intensities with increasing n reflects the gradual closing of the fragmentation channel.

For $n=1$, the O^- and NO^- photofragments are attributed to the dissociations of NNO_2^- and $ONNO^-$, respectively. The intense O^- signal in the fragment mass spectrum complements the assignment the O^- band (feature I) in photoelectron spectrum 1.1 to the photodetachment of the O^- photofragment of NNO_2^-. The fragmentation results are therefore consistent with a predominance of the NNO_2^- parent-anion structure for $n=1$.

For $n \geq 2$, the dominant peak in each of the photofragment-ion mass spectra corresponds to $[O(N_2O)]^-$ ($m/z=60$). This fragment anion can be formed via at least two different mechanisms. (1) A secondary reaction of the nascent O^- photoproduct of the NNO_2^- cluster core with a N_2O solvent molecule to form a hot $N_2O_2^-$ anion, which may relax by evaporation of any remaining N_2O molecules. (2) Photoexcitation of the NNO_2^- cluster core, which then internally converts to the ground electronic state, leading to cluster predissociation via the loss of solvent molecules. Our work on the photofragmentation of $NNO_2^-(H_2O)$ shows that the main photofragment in that case is also $[O(N_2O)]^-$ or $N_2O_2^-$, with a branching ratio of ~96% and the remaining fraction accounting for the smaller contributions from O^- and $O^-(H_2O)$.[42] This result rules out the nascent O^- reaction with the solvent and provides a solid indication that predissociation (following the electronic excitation of the cluster core) is an effective fragmentation mechanism for the NNO_2^- based clusters. This observation echoes with the work of Bowers and co-workers[43,44] for the photodissociation of $CO_3^-(H_2O)$, where they reported a cross section for the CO_3^- product that was 31 times greater than that for the $O^-(H_2O)$ fragment. (The CO_3^- fragmentation channel was also explained by means of vibrational predissociation).[44]

The $N_2O_2^-$ fragment persists through $n=7$, with no observable contributions from $N_2O_2^-(N_2O)_k$, $k>0$. Within either of the two above mechanisms of its appearance, the $N_2O_2^-$ photofragment is a signature of the $N_2O_2^-$ covalent core in the parent cluster. Therefore, the most important aspect of the fragmentation results is the conspicuous drop in the $N_2O_2^-$ yield between $n=3$ and $n=4$, which continues with increasing n until its complete disappearance after $n=7$. This decrease in the $N_2O_2^-$ channel (and, therefore, the overall fragmentation yield) reflects a diminishing fraction of the parent clusters with a covalent $N_2O_2^-$ core over a growing fraction of clusters with an atomic O^- core, which are responsible for the strong photodetachment signals observed for $n \geq 4$. These results complement the photoelectron imaging data in the sense that some degree of coexistence between the atomic and molecular cluster cores is shown to persist over a small range of cluster sizes. More importantly, the two experiments concur in that the main transition from a molecular cluster core to an atomic core occurs between $n=3$ and $n=4$.

IV. DISCUSSION

The present study is the first investigation of the $[O(N_2O)_n]^-$ cluster series in the size range up to $n=9$ via photoelectron spectroscopy. The experimental results reveal a transition from the molecular (NNO_2^-) to atomic (O^-) cluster core structure occurring between $n=3$ and 4. Although both core types may coexist, to a degree, through the entire cluster size range studied, an overwhelming predominance of clusters with the molecular core is seen for $n=1-3$, while the atomic anion based clusters clearly dominate for $n=4-9$. Accordingly, the $[O(N_2O)_n]^-$ anion population can be described as a combination of the competing distributions of the $NNO_2^-(N_2O)_{n-1}$ and $O^-(N_2O)_n$ clusters. Judging by the signal levels, the $NNO_2^-(N_2O)_{n-1}$ distribution peaks at $n=1$ and decreases as the cluster size increases, with a very quick falloff after $n=3$ where the $O^-(N_2O)_n$ series emerges.

The core-switching phenomenon is expected to depend on the relative stabilities of the $O^-(N_2O)_n$ and $NNO_2^-(N_2O)_{n-1}$ cluster anions. For $n=1$, covalent bonding in NNO_2^- is energetically favored over the solvation of O^- by N_2O. However, O^- should be solvated more effectively than NNO_2^- due to the more localized charge of the atomic anion. As the number of solvent molecules increases, the difference between the solvent stabilization energies for $O^-(N_2O)_n$ and $NNO_2^-(N_2O)_{n-1}$ may exceed the extra covalent bond energy in NNO_2^-, making the O^--based clusters more favorable energetically. Similar arguments were made previously for the core switching in $(CO_2)_n^-$.[4,5,45]

The relative stabilities of the $NNO_2^-(N_2O)_{n-1}$ and $O^-(N_2O)_n$ clusters, ΔE_n, can be estimated from the solvent evaporation and bond dissociation energies and expressed approximately as[46]

$$\Delta E_n = D_0(NNO_2^-) + \Delta_{n-1}\mathrm{VDE}(NNO_2^-) - \Delta_n \mathrm{VDE}(O^-). \quad (1)$$

In Eq. (1), $D_0(NNO_2^-)$ is the $NNO_2^- \rightarrow O^- + N_2O$ bond dissociation energy, while $\Delta_{n-1}\mathrm{VDE}(NNO_2^-)$ and $\Delta_n \mathrm{VDE}(O^-)$ are

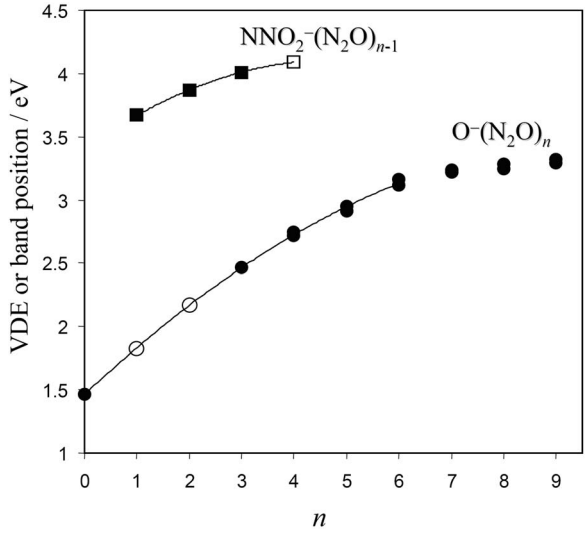

FIG. 3. The detachment energies of bands III and IV (peak a) for the $O^-(N_2O)_n$ and $NNO_2^-(N_2O)_{n-1}$ cluster anions, respectively. The corresponding bands appear in the photoelectron spectra in Figs. 1 and 2. The solid symbols indicate the direct experimental results, while the open symbols show the interpolated or extrapolated "missing" values.

the shifts in the NNO_2^- and O^- photoelectron band positions due to the interaction with $(n-1)$ and n N_2O solvent molecules, respectively. Specifically,

$$\Delta_{n-1}\mathrm{VDE}(NNO_2^-) = \mathrm{VDE}[NNO_2^-(N_2O)_{n-1}] - \mathrm{VDE}[NNO_2], \quad (2)$$

$$\Delta_n\mathrm{VDE}(O^-) = \mathrm{VDE}[O^-(N_2O)_n] - \mathrm{VDE}[O^-], \quad (3)$$

The determination of relative stabilities using Eq. (1) is based on several approximations. In particular, while assuming that solvent evaporation energy is implicit in the VDE shifts, we neglect the clustering energies on the corresponding neutral surfaces. In determining $\Delta_{n-1}\mathrm{VDE}(NNO_2^-)$, we will use the solvation-induced shift of band IV's peak *a* identified in Figs. 2.1–2.3.

Two independent measurements of the $NNO_2^- \rightarrow O^- + N_2O$ dissociation are available in the literature, giving the rather disparate $D_0(NNO_2^-)$ values of 1.40 ± 0.03 eV (Ref. 13) and 0.57 ± 0.05 eV.[14] In both cases, the dissociation energy is determined from the maximum fragment kinetic energy release in the dissociative photodetachment of NNO_2^-, but via two different pathways: $O(^3P) + N_2O + e^-$ at 532 nm in Ref. 13 and $N(^4S) + NO_2 + e^-$ at 266 nm in Ref. 14. The latter channel has a better Franck–Condon overlap with the parent NNO_2^- owing to the bent equilibrium geometry of NO_2. It is therefore expected to yield a less excited NO_2 photofragment (compared to N_2O in the other channel) and provide a more accurate determination of $D_0(NNO_2^-)$.

Although the VDEs for both the O^- and NNO_2^- cluster core types are not available for all cluster sizes studied due to the size-dependent core preference, we have estimated the "missing" VDE values by interpolating or extrapolating the observed band positions for the series of each core type. Figure 3 displays plots of the cluster-size-dependent detachment energies for $O^-(N_2O)_n$ and $NNO_2^-(N_2O)_{n-1}$, determined from bands III and IV (peak *a*), respectively. The solid symbols indicate the direct experimental results, while the open symbols show the interpolated or extrapolated missing values.

TABLE I. Relative stabilities (ΔE_n/eV) of the $NNO_2^-(N_2O)_{n-1}$ and $O^-(N_2O)_n$ cluster anions. Positive ΔE_n values indicate that the corresponding NNO_2^- based clusters are more stable than those with the O^- core.

n	Experiment[a]	Experiment[b]	MP2[c]	CCSD[d]	CCSD[e]
1	1.03	0.20	0.33	1.01	0.98
2	0.89	0.06	0.24	0.91	⋯
3	0.73	−0.10	⋯	⋯	⋯
4	0.56	−0.29	≤0.07	≤0.62	⋯

[a]Based on the value of $D_0(NNO_2^-) = 1.40 \pm 0.03$ eV by Osborn *et al.* (Ref. 13).
[b]Based on the value of $D_0(NNO_2^-) = 0.57 \pm 0.05$ eV by Li *et al.* (Ref. 14).
[c]UMP2/aug-cc-pVDZ.
[d]CCSD/6-31+G*//MP2/aug-cc-pVDZ.
[e]CCSD/aug-cc-pVDZ.

Since the solvent-induced shift in the VDE between $n-1$ and n is approximately equal to the binding energy of the nth solvent molecule to the cluster, we estimate that the sequential binding energies of the first, second, third, and fourth N_2O's to O^- are 0.37, 0.34, 0.30, and 0.25 eV, respectively. These numbers are strikingly close to the corresponding values of 0.37, 0.34, 0.30, and 0.28 eV for the sequential binding energies of N_2O to OH^- determined previously by Kim *et al.*[47]

From the data summarized in Fig. 3 and the two aforementioned values of $D_0(NNO_2^-)$, the relative stabilities of the $O^-(N_2O)_n$ and $NNO_2^-(N_2O)_{n-1}$ cluster anions can be calculated using Eq. (1). The relative stabilities calculated using each literature value of D_0 are listed in Table I. Positive ΔE_n indicate that the corresponding NNO_2^- based clusters are more stable than those with the O^- core. The estimated ΔE_n values based on $D_0 = 1.40$ eV (first column in Table I) suggest that from the thermodynamic standpoint, the $NNO_2^- \rightarrow O^-$ core switching should not happen at $n=4$, where our experimental data clearly indicate that the O^- based clusters become the predominant species. However, the relative stabilities calculated using $D_0 = 0.57$ eV (second column in Table I) do show that the core switching should occur at around $n=3$, which agrees well with the first appearance of the type III transitions at this cluster size in our experiment.

It is also instructive to compare the experimental estimates of the relative stabilities for the $[O(N_2O)_n]^-$ series with theoretical predictions. To elucidate the relative stabilities of the cluster isomers, *ab initio* calculations were carried out for $O^-(N_2O)_n$ and $NNO_2^-(N_2O)_{n-1}$, $n=1-4$, using the GAUSSIAN 03 program package.[48] The geometries were optimized at the unrestricted second-order Møller-Plesset perturbation theory (UMP2/aug-cc-pVDZ) level, followed by harmonic frequency calculations at the same theory level to verify that the stationary points found correspond to true potential minima. The computed energies were corrected for zero-point vibrational energies and basis set superposition errors.[49]

The Hartree–Fock (HF) wave functions for all $[O(N_2O)_n]^-$, $n=1-4$ structures, except for NNO_2^-, possess

internal instabilities,[50,51] which can lead to oscillatory behavior during geometry optimization and symmetry breaking in the nuclear framework.[52] In addition, the Møller–Plesset energies based on unstable wave functions are also questionable. Therefore, the MP2 results should be viewed as mere estimates to compare to the experimental findings. For $n=1$, in addition to the NNO_2^- global minimum,[13,53] we find a shallow potential minimum corresponding to a planar $O^-\cdot N_2O$ ion-molecule complex, in which the N_2O is bent at 173.4°. The number of structural isomers increases with the cluster size. We found five stable $[O(N_2O)_2]^-$ structures: three with the NNO_2^- cluster core and two with the O^- core. In the calculations for $n=3-4$ clusters, we did not locate any potential minima corresponding to O^- based structures. In the case of $O^-(N_2O)_3$, the energies oscillate and the geometry optimization does not converge. For $O^-(N_2O)_4$, we found one stationary point, which is a first-order saddle point corresponding to the structure of D_2 symmetry.

In general, the instability of a HF wave function indicates that the independent particle approximation breaks down and there is a broken symmetry solution with lower energy. Thus, a more sophisticated computational model with higher electron correlation and/or multireference approach[54] is necessary for an adequate description of such species. It has been shown that coupled-cluster (CC) methods can be successfully applied to treat the instability problem,[55–57] provided that the system can be described by a single configuration wave function. The CC calculations with single and double excitations (at the CCSD/6-31+G*//MP2/aug-cc-pVDZ level) were carried out for some of the cluster structures of interest. Since the geometries and the energies of the clusters can be quite different depending on the particular method and basis set employed in the calculations, for the comparison to CCSD/6-31+G*//MP2/aug-cc-pVDZ results, the geometry optimizations followed by frequency calculations were also performed at the CCSD/aug-cc-pVDZ for $n=1$ species. No instabilities are detected for the wave functions with the CC calculations.

The relative stabilities ΔE_n defined as the energy differences between the most stable $O^-(N_2O)_n$ and $NNO_2^-(N_2O)_{n-1}$ structures computed from MP2 and CC results are summarized in the last three columns of Table I. Although both the MP2 and CC calculations find that NNO_2^- is more stable than $O^-\cdot N_2O$, there is a significant discrepancy in the computed relative energies: MP2 estimates that NNO_2^- is more stable by a mere 0.33 eV, while CC methods yield a difference of about 1 eV. Nonetheless, both the MP2 and CC energies are consistent with the lack of $O^-\cdot N_2O$ signatures in the experimental data (Figs. 1.1 and 2.1). The relative stabilities determined by both the MP2 and CC methods indicate that the energy difference between the $O^-(N_2O)_n$ and $NNO_2^-(N_2O)_{n-1}$ clusters decreases steadily with increasing n, which is consistent with the assumption of O^- being solvated more effectively than NNO_2^- and is necessary for the core switching to occur. However, both the MP2 and CC methods predict that the NNO_2^- based species remain favored energetically even for $n=4$, where the experiment indicates a nearly complete switch to the O^- core type.

Specifically, MP2 predicts the $NNO_2^-(N_2O)_3$ to be more stable than $O^-(N_2O)_4$ by only 0.07 eV, while the CCSD/6-31+G*//MP2/aug-cc-pVDZ estimates a 0.62 eV difference. We note also that MP2 provides a better quantitative agreement with the estimates of ΔE_n based on $D_0(NNO_2^-)=0.57$ eV,[14] which are in accord with the present experimental observations. The CC calculations closely match the relative stabilities based on the 1.40 eV value of $D_0(NNO_2^-)$,[13] which are not in agreement with the present experimental results. This outcome is surprising, since one should not expect MP2 performance to be superior to the CC methods, especially given the wave function instability problems discussed above. Therefore, the observed agreement of the MP2 results with the experiment is likely serendipitous.

To conclude, we have obtained two sets of relative stabilities ΔE_n of the $NNO_2^-(N_2O)_{n-1}$ versus $O^-(N_2O)_n$ cluster structures, summarized in columns 1 and 2 of Table I. Per Eq. (1), these estimates are based on our own experimental data and the two available (yet drastically different) measurements of the NNO_2^- bond dissociation energy. One of the ΔE_n series supports and the other contradicts the simple thermodynamic model of the experimentally observed NNO_2^- to O^- core switching. Although the present experimental results are compelling, the discrepancies between past experimental measurements and theoretical models call for caution in concluding that the suggested thermodynamic mechanism is the only possible explanation for the observed core switching. Alternatively, it could be possible for the larger clusters ($n\geq 4$) to be formed initially with the O^- core and remain trapped in the corresponding (possibly metastable) state on the timescale of our experiment (tens of microseconds). Such kinetic model would imply the existence of a barrier for the association reaction of O^- with any one of the surrounding N_2O solvent molecules. Certainly, additional experimental data on NNO_2^- bond dissociation energy would help to draw a confident conclusion on the core-switching mechanism. At present, the work of Li and Continetti[14] is believed to provide more accurate determination of $D_0(NNO_2^-)$, supporting the thermodynamic picture of the core switching reported here.

V. SUMMARY

Photoelectron imaging experiments on $[O(N_2O)_n]^-$, $n=0-9$, at 266 and 355 nm provide clear evidence of a switch from the covalent NNO_2^- cluster core to the atomic O^- core occurring between $n=3$ and 4. Although there is some coexistence between the molecular (NNO_2^- and some $ONNO^-$) and atomic (O^-) core structures, the results suggest an overwhelming predominance of the Y-shaped NNO_2^- cluster core structure for $n=1-3$ and the atomic O^- core for $n>3$. The core switching is explained in terms of a simple thermodynamic model based on the relative stabilities of the $O^-(N_2O)_n$ and $NNO_2^-(N_2O)_{n-1}$ cluster anions. The model argues that despite the greater stability of NNO_2^- relative to the $O^-+N_2O^-$ dissociation limit, an O^- cluster core becomes energetically favored over NNO_2^- for $n>3$ due to the more effective solvation of the atomic anion. Within this thermo-

dynamic picture, the present results lend indirect support to the past measurement of NNO_2^- bond dissociation energy by Li and Continetti.[14]

ACKNOWLEDGMENTS

The financial support for this work is provided by the National Science Foundation (Grant No. CHE-0713880), the Lucile and David Packard Foundation (Packard Fellowship for Science and Engineering), and the ACS Petroleum Research Fund (Grant No. 45406-AC6).

[1] A. W. Castleman and K. H. Bowen, J. Phys. Chem. **100**, 12911 (1996).
[2] A. Sanov and W. C. Lineberger, Phys. Chem. Chem. Phys. **6**, 2018 (2004).
[3] I. Yourshaw, Y. X. Zhao, and D. M. Neumark, J. Chem. Phys. **105**, 351 (1996).
[4] M. J. DeLuca, B. Niu, and M. A. Johnson, J. Chem. Phys. **88**, 5857 (1988).
[5] T. Tsukuda, M. A. Johnson, and T. Nagata, Chem. Phys. Lett. **268**, 429 (1997).
[6] S. H. Fleischman and K. D. Jordan, J. Phys. Chem. **91**, 1300 (1987).
[7] T. Tsukuda, M. Saeki, L. Zhu, and T. Nagata, Chem. Phys. Lett. **295**, 416 (1998).
[8] L. A. Posey and M. A. Johnson, J. Chem. Phys. **88**, 5383 (1988).
[9] J. Hacaloglu, S. Suzer, and L. Andrews, J. Phys. Chem. **94**, 1759 (1990).
[10] M. E. Jacox, J. Chem. Phys. **93**, 7622 (1990).
[11] M. E. Jacox and W. E. Thompson, J. Chem. Phys. **93**, 7609 (1990).
[12] D. W. Arnold and D. M. Neumark, J. Chem. Phys. **102**, 7035 (1995).
[13] D. L. Osborn, D. J. Leahy, D. R. Cyr, and D. M. Neumark, J. Chem. Phys. **104**, 5026 (1996).
[14] R. J. Li and R. E. Continetti, J. Phys. Chem. A **106**, 1183 (2002).
[15] J. M. Warman, R. W. Fessenden, and G. Bakale, J. Chem. Phys. **57**, 2702 (1972).
[16] C. E. Klots and R. N. Compton, J. Chem. Phys. **69**, 1636 (1978).
[17] M. Knapp, O. Echt, D. Kreisle, T. D. Mark, and E. Recknagel, Chem. Phys. Lett. **126**, 225 (1986).
[18] Z. Sojka and M. Che, J. Phys. Chem. **100**, 14776 (1996).
[19] A. D. Bass, M. Lezius, P. Ayotte, L. Parenteau, P. Cloutier, and L. Sanche, J. Phys. B **30**, 3527 (1997).
[20] J. M. Weber, E. Leber, M. W. Ruf, and H. Hotop, Phys. Rev. Lett. **82**, 516 (1999).
[21] E. Leber, S. Barsotti, J. Bommels, J. M. Weber, I. I. Fabrikant, M. W. Ruf, and H. Hotop, Chem. Phys. Lett. **325**, 345 (2000).
[22] E. S. Kryachko, C. Vinckier, and M. T. Nguyen, J. Chem. Phys. **114**, 7911 (2001).
[23] H. U. Suter and T. Greber, J. Phys. Chem. B **108**, 14511 (2004).
[24] G. Hanel, T. Fiegele, A. Stamatovic, and T. D. Mark, Int. J. Mass. Spectrom. **205**, 65 (2001).
[25] K. Hiraoka, S. Fujimaki, K. Aruga, and S. Yamabe, J. Phys. Chem. **98**, 8295 (1994).
[26] S. Yamamoto, K. Mitsuke, F. Misaizu, T. Kondow, and K. Kuchitsu, J. Phys. Chem. **94**, 8250 (1990).
[27] R. Mabbs, E. Surber, and A. Sanov, Analyst (Cambridge, U.K.) **128**, 765 (2003).
[28] A. Sanov and R. Mabbs, Int. Rev. Phys. Chem. **27**, 53 (2008).
[29] E. Surber, R. Mabbs, and A. Sanov, J. Phys. Chem. A **107**, 8215 (2003).
[30] M. A. Johnson and W. C. Lineberger, in *Techniques for the Study of Ion Molecule Reactions*, edited by J. M. Farrar and W. H. Saunders (Wiley, New York, 1988), p. 591.
[31] A. T. J. B. Eppink and D. H. Parker, Rev. Sci. Instrum. **68**, 3477 (1997).
[32] D. W. Chandler and P. L. Houston, J. Chem. Phys. **87**, 1445 (1987).
[33] W. H. Robertson, J. A. Kelley, and M. A. Johnson, Rev. Sci. Instrum. **71**, 4431 (2000).
[34] W. C. Wiley and I. H. McLaren, Rev. Sci. Instrum. **26**, 1150 (1955).
[35] E. Surber, S. P. Ananthavel, and A. Sanov, J. Chem. Phys. **116**, 1920 (2002).
[36] A. J. R. Heck and D. W. Chandler, Annu. Rev. Phys. Chem. **46**, 335 (1995).
[37] V. Dribinski, A. Ossadtchi, V. A. Mandelshtam, and H. Reisler, Rev. Sci. Instrum. **73**, 2634 (2002).
[38] L. Velarde, T. Habteyes, and A. Sanov, J. Chem. Phys. **125**, 114303 (2006).
[39] D. M. Neumark, K. R. Lykke, T. Andersen, and W. C. Lineberger, Phys. Rev. A **32**, 1890 (1985).
[40] S. J. Cavanagh, S. T. Gibson, M. N. Gale, C. J. Dedman, E. H. Roberts, and B. R. Lewis, Phys. Rev. A **76**, 052708 (2007).
[41] L. Velarde, T. Habteyes, E. Grumbling, K. Pichugin, and A. Sanov, J. Chem. Phys. **127**, 084302 (2007).
[42] L. Velarde, Ph.D. thesis, University of Arizona, 2008.
[43] J. T. Snodgrass, H. S. Kim, and M. T. Bowers, J. Chem. Phys. **88**, 3072 (1988).
[44] C. M. Roehl, J. T. Snodgrass, C. A. Deakyne, and M. T. Bowers, J. Chem. Phys. **94**, 6546 (1991).
[45] J. W. Shin, N. I. Hammer, M. A. Johnson, H. Schneider, A. Gloss, and J. M. Weber, J. Phys. Chem. A **109**, 3146 (2005).
[46] S. Roszak and J. Leszczynski, *Computational Chemistry* (World Scientific, Singapore, 2001), Vol. 6, p. 179.
[47] J. B. Kim, P. G. Wenthold, and W. C. Lineberger, J. Chem. Phys. **108**, 830 (1998).
[48] M. J. Frisch *et al.*, GAUSSIAN 03, Gaussian, Inc., Wallingford CT, 2004.
[49] S. F. Boys and F. Bernardi, Mol. Phys. **19**, 553 (1970).
[50] R. Seeger and J. A. Pople, J. Chem. Phys. **66**, 3045 (1977).
[51] H. Fukutome, Int. J. Quantum Chem. **20**, 955 (1981).
[52] J. Paldus and A. Veillard, Mol. Phys. **35**, 445 (1978).
[53] A. Snis and I. Panas, Chem. Phys. **221**, 1 (1997).
[54] M. S. Gordon, M. W. Schmidt, G. M. Chaban, K. R. Glaesemann, W. J. Stevens, and C. Gonzalez, J. Chem. Phys. **110**, 4199 (1999).
[55] P. D. Hiberty, in *Modern Electronic Structure Theory and Applications in Organic Chemistry*, edited by R. D. Ernest (World Scientific, Singapore, 1997), p. 320.
[56] P. G. Szalay, J. Vazquez, C. Simmons, and J. F. Stanton, J. Chem. Phys. **121**, 7624 (2004).
[57] T. Pasinszki, Phys. Chem. Chem. Phys. **10**, 1411 (2008).